Pergamon

SCIENCE DIRECT®

Tetrahedron 59 (2003) 5719–5730

TETRAHEDRON

Photoinduced electron transfer reaction tuned by donor–acceptor pairs via the rigid, linear spacer heptacyclo[6.6.0.0^{2,6}.0^{3,13}.0^{4,11}.0^{5,9}.0^{10,14}]tetradecane

Tahsin J. Chow,[a,*] Nan-Rong Chiu,[a] Hong-Chuan Chen,[a] Chong-Yow Chen,[b] Wei-Shan Yu,[c] Yi-Ming Cheng,[c] Chung-Chih Cheng,[d] Chen-Pin Chang[d] and Pi-Tai Chou[c,*]

[a]*Institute of Chemistry, Academia Sinica, Taipei 115, Taiwan, ROC*
[b]*Department of Chemistry, National Chung Cheng University, Chia-Yi 621, Taiwan, ROC*
[c]*Department of Chemistry, National Taiwan University, Taipei 106, Taiwan, ROC*
[d]*Department of Chemistry, Fu-Jen Catholic University, Taipei 242, Taiwan, ROC*

Received 19 December 2002; revised 10 April 2003; accepted 30 May 2003

Abstract—A new class of donor-{saturated hydrocarbon bridge}-acceptor (D–B–A) dyads were synthesized and utilized on a systematic approach to evaluate the corresponding photoinduced electron transfer (ET) process. Among these dyads heptacyclo[6.6.0.0^{2,6}.0^{3,13}.0^{4,11}.0^{5,9}.0^{10,14}]tetradecane (HCTD) was used as a unique spacer, which possesses a geometry of high symmetry (D_{2d}), rigidity and linearity. The spectroscopy and dynamics of excited-state ET as functions of donor/acceptor electronic states, orientation as well as solvent properties were analyzed with the aid of theoretical computations. It was observed that the quenching of donor fluorescence (the F_1 band) correlated with the appearance of a broad charge-transfer (CT) emission. Both wavelength and intensity of the CT band varied with solvent-polarity, whereas its rise dynamics complied well with the decay of the F_1 band. In acetonitrile, the CT state decays much faster than the rate of ET ($\sim$63 ps^{-1}) so that the corresponding steady-state emission cannot be resolved. An intriguing effect was observed in the case of benzene-1,2-dithioketals (**3a** and **3b**) where the D and A π-chromophores were aligned in different orientations. The estimated ET rate of **3a** (3.9×10^{10} s^{-1}) was substantially faster than that of **3b** (7×10^{8} s^{-1}). The experimental data were tentatively fitted by a semi-log plot of ET rate constants (k_{et}) against free energy (ΔG^0), yielding a value of $\sim$17.3 cm^{-1} for the electron-coupling matrix (H_{el}).

1. Introduction

Electron transfer represents one of the most fundamental pathways in many physical and biological processes.[1] On one hand, biological and modified biological systems contain a variety of redox centers at widely different distances, among which electron transfer occurs on a time scale from the picosecond region to many seconds.[2–11] On the other hand, through synthetic efforts, long range intramolecular electron/hole transfer between rigid, covalently linked electron donor-{saturated hydrocarbon bridge}-acceptor (D–B–A) dyads have served as heuristic models of biological electron transfer and/or photosynthesis.[12–17] From the viewpoint of application, knowledge collected in the photoinduced electron process is important in the design of molecular devices, such as molecular rectifiers,[18–21] switches,[22,23] electrochemical sensors,[24,25] photovoltaic cells,[13b,26] and nonlinear optical materials.[27,28] An ideal device requires an ingenious molecular spacer between the donor (D) and the acceptor (A) chromophores, so that the flow of electrons can be regulated in a controlled manner.[29,30]

In our previous communication a new rod-shaped molecule heptacyclo[6.6.0.0^{2,6}.0^{3,13}.0^{4,11}.0^{5,9}.0^{10,14}]tetra-decane (HCTD, see Fig. 1) has been synthesized and applied as a spacer group for electron transfer processes between a donor (D) and an acceptor (A) substituents.[31,32] The geometry of HCTD has the virtue of high symmetry (D_{2d}) as well as structural rigidity, leading to the feasibility of aligning the donor and acceptor chromophores linearly across a σ-skeleton. Thus, the entire D–B–A frame possesses a mirror plane symmetry element. Furthermore, the relative orientation between donor and acceptor can be adjusted to allow their π-orbitals to be either coplanar (0°) or perpendicular (90°) in dihedral angle with respect to each other. In the present work comprehensive steady state and time-resolved fluorescence studies were incorporated to systematically investigate the dependence of the rate of electron transfer as functions of D/A and solvent properties. Our goal is aimed at utilizing the newly developed linear

Keywords: photoinduced electron transfer; dual fluorescence; linear HCTD spacer.
* Corresponding authors. Tel.: +886-2-27898552; fax: +886-2-27884179; e-mail: tjchow@chem.sinica.edu.rw

0040–4020/$ - see front matter © 2003 Elsevier Ltd. All rights reserved.
doi:10.1016/S0040-4020(03)00881-0

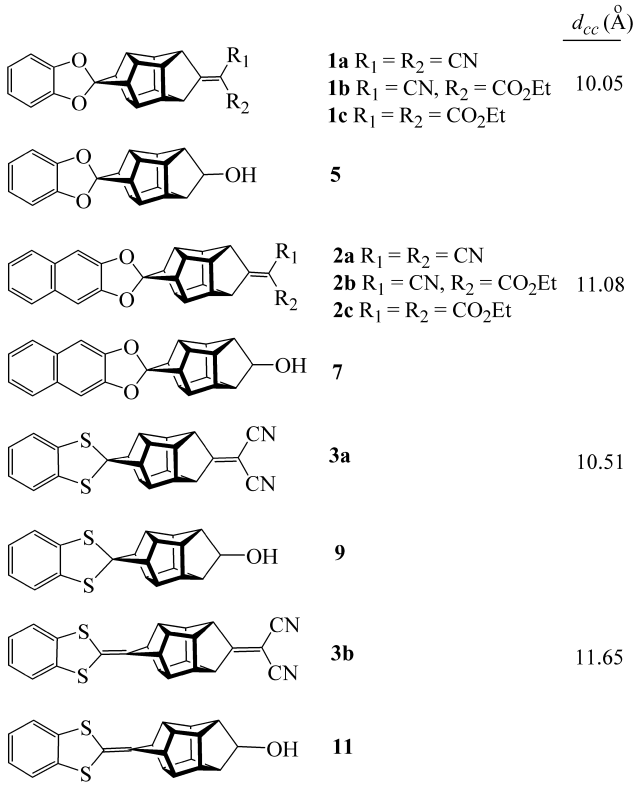

Figure 1. Structures of various D–B–A systems and their corresponding nonelectron-transfer models. d_{cc} is the center-to-center distance between the donor and acceptor.

HCTD spacer to gain an insight into the factors controlling long distance electron transfer, in particular the effect of reaction thermodynamics.

2. Results

For clarity, structures of the studied D–B–A systems **1a**-**c**, **2a**-**c** and **3a**,**b** are depicted in Figure 1. A standard procedure for the preparation of **1a** is outlined in Scheme 1. The catechol ketal **5** was made from **4** in 94% yields by dehydration upon the catalysis of *p*-toluenesulfonic acid. Oxidation of **5** with pyridinium chlorochromate (PCC) gave ketone **6** in 89% yield. The ^{13}C NMR spectrum of **6** shows the characteristics of C_{2v} symmetry, i.e. nine absorption lines appeared in ^{13}C NMR and five in ^{1}H fields. Starting from precursor **6**, compounds **1a**-**c** were prepared by base-catalyzed condensation reactions with malononitrile, ethyl 2-cyanoacetate and diethyl malonate, respectively. The preparation of **2a**-**c** with a naphthalene moiety followed a similar reaction sequence via an alcohol **7** and ketone **8**. For systems **1a**-**c** and **2a**-**c**, the π-orbitals between donor and acceptor chromophores are coplanar. In another approach, **3a** and **3b** (see Fig. 1) were synthesized, in which the orientation of π-orbitals interaction between donor and acceptor is in parallel and perpendicular configuration, respectively (see Section 5 for details).

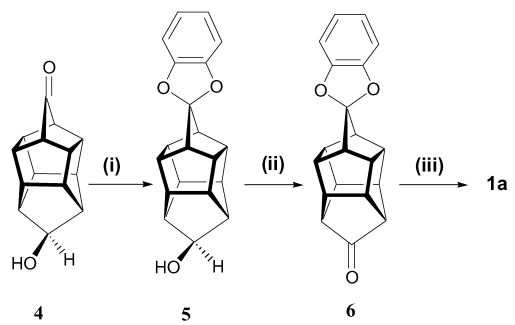

Scheme 1. *Reagents*: (i) catechol, *p*-toluenesulfonic acid (catalytic), benzene reflux, 94% yield; (ii) PCC, CH_2Cl_2, 89% yield; (iii) malononitrile, AcOH, β-analine, benzene reflux, 94% yield.

2.1. Steady-state spectroscopy

To simplify the results and discussion, a series of naphthalene related systems, i.e. **2a**-**c** and **7**, were mainly used as prototypes to demonstrate the UV–Vis/fluorescence properties and their corresponding spectral analyses. Accordingly, spectroscopic and dynamic data of the remaining systems can be referred to in Tables 1 and 2. For **2a**-**c**, due to their similarity to **7** by virtue of the presence of the naphthalene moiety, the characteristic $\pi\pi^*$ absorption profile with vibronic progressions at >280 nm in

Table 1. Steady state UV/Vis and fluorescence parameters at 298 K

	Abs. λ_{max}. (nm)	em. F_1 λ_{max}. (nm)	em. CT λ_{max}. (nm)	Φ_f	Φ_{CT}
1a	283	316[a]	500[a]	7.68×10^{-4}	1.87×0^{-3}
		316[b]	528[b]	3.27×10^{-4}	1.56×10^{-3}
		316[c]	–	7.64×10^{-4}	–
1b	283	316[a]	485[a]	4.66×10^{-4}	2.24×10^{-3}
		316[b]	496[b]	2.21×10^{-4}	2.00×10^{-3}
		316[c]	–	2.68×10^{-4}	–
1c	283	316[a]	458[a]	1.59×10^{-2}	4.95×10^{-3}
		318[b]	472[b]	1.01×10^{-2}	4.52×10^{-3}
		316[c]	–	6.54×10^{-3}	–
5	286	312[a]	–	1.74×10^{-1}	
		312[b]		1.63×10^{-1}	
		312[c]		1.55×10^{-1}	
2a	326	328[a]	481[a]	9.65×10^{-3}	1.08×10^{-2}
		329[b]	506[b]	4.04×10^{-3}	4.72×10^{-3}
		328[c]	–	3.57×10^{-3}	–
2b	326	329[a]	454[a]	5.71×10^{-2}	2.83×10^{-2}
		328[b]	485[b]	1.19×10^{-2}	7.85×10^{-3}
		329[c]	–	1.05×10^{-2}	–
2c	326	329[a]	–	3.25×10^{-1}	–
		328[b]	–	3.32×10^{-1}	–
		329[c]	–	3.39×10^{-1}	–
7	327	328[a]		3.50×10^{-1}	
		328[b]		3.49×10^{-1}	
		328[c]		3.46×10^{-1}	
3a	276	365[a,d]	518[a]	1.54×10^{-4}	3.16×10^{-3}
		365[b,d]	542[b]	–	2.21×10^{-3}
9	281	360[a,d]	–		–
3b	318	413[a,d]	–	1.5×10^{-4}	–
		413[b,d]	–		
		413[c,d]	–		
11	316	410[a,d]	–		–

[a] In THF.
[b] In DCM.
[c] In ACN.
[d] Extremely weak steady-state emission was detected by the laser induced fluorescence.

Table 2. Fluorescence lifetime (τ) and calculated reaction free energy (ΔG^0) in various solvents

	THF				CH_2Cl_2				CH_3CN			
	F_1 τ (ns)	CT τ (ns)	k_{et} 10^{10} s^{-1}	ΔG^0 (eV)	F_1 τ (ns)	CT τ (ns)	k_{et} 10^{10} s^{-1}	ΔG^0 (eV)	F_1 τ (ns)	CT τ (ns)	k_{et} 10^{10} s^{-1}	ΔG^0 (eV)
1a	0.02	0.03 (−4.5)[a] 0.11 (4.6)	4.97	−0.91	0.02	0.02 (−5.7) 0.11 (6.2)	5.52	−0.96	0.01	0.02	8.29	−1.99
1b	0.03	0.03 (−5.0) 0.18 (5.0)	3.25	−0.84	0.03	0.03 (−6.0) 0.14 (7.0)	3.81	−0.88	0.02	0.01	6.21	−1.03
1c	0.23	0.21 (−4.7) 0.47 (5.5)	0.40	−0.51	0.09	0.08 (−5.0) 0.34 (5.8)	1.14	−0.55	0.12	0.10	0.79	−0.69
5	2.90				2.80				2.60			
2a	0.11	0.11 (−1.8) 1.69 (2.1)	0.94	−0.23	0.02	0.02 (−1.7) 0.71 (2.1)	6.24	−0.28	0.07	0.06	1.42	−0.44
2b	0.57	0.59 (−3.7) 2.05 (4.3)	0.17	−0.16	0.18	0.20 (−3.0) 0.77 (3.3)	0.55	−0.20	0.25	0.23	0.39	−0.35
2c	10.47	–	–	0.17	10.30	–	–	0.13	10.30	–	–	−0.01
7	10.70				10.66				10.64			
3a	0.02	0.02 (−4.8) 2.00 (5.5)	3.90	−1.09	0.08	0.08 (−5.0) 0.51 (5.7)	0.12	−1.14	0.06	0.07	0.66	−1.31
9	0.09				0.09				0.09			
3b	0.10	–	0.07	−1.03	0.10	–	0.07	−1.09	0.10	–	0.05	−1.26
11	0.11				0.11				0.11			

[a] The numbers in the parenthesis ( )$\times 10^{-2}$ are pre-exponential factor of Eq. (3). Note the negative sign corresponds to a rise component.

tetrahydrofuran (THF) can unambiguously be ascribed to low lying energy bands (^1L_a and ^1L_b) of the naphthalendiol ketal moiety. Similar absorption features were obtained in other solvents such as dichloromethane (DCM) and acetonitrile (ACN. see Table 1), indicating that the interaction between D and A groups through the HCTD spacer is negligible in the ground electronic state. Figure 2 shows room temperature emission spectra of **2a**-**c** in three solvents examined. For **2a** and **2b** dual emission specified as F_1 (the short-wavelength emission) and CT bands were clearly observed in THF and DCM. Owing to the overlap of the 0–0 onset with its corresponding $S_0 \rightarrow S_1$ ($\pi\pi^*$) absorption, the assignment of the F_1 band to the normal Stokes shifted emission of the naphthalendiol moiety is apparent. The intensity ratio for the CT versus the F_1 band is concentration independent. In addition, the excitation spectra monitored at F_1 and CT bands are effectively identical, indicating that both emissions originate from the same ground state precursor. In a comparative study, compound **7**, which only possesses a naphthalendiol moiety coupled with the HCTD spacer and is considered a nonelectron-transfer model for compound **2** series, exhibits a unique fluorescence band maximum at ~330 nm (i.e. the F_1 band) in all solvents studied. In comparison to **7**, remarkable quenching of the F_1 band was readily perceived in **2a**-**b** through its emission intensity. The apparent quantum yields (Φ_f) were measured to be 9.65×10^{-3} and 5.71×10^{-2} for **2a** and **2b**, respectively, which are far lower than that of 3.50×10^{-1} for **7** in THF. Φ_f for the F_1 band are also low for **2a** and **2b** in DCM and ACN (see Table 1), while similar high Φ_f values of 3.49×10^{-1} and 3.46×10^{-1} were obtained for **7**. In contrast, the quenching of the F_1 intensity is negligibly small in the case of **2c**, as indicated by Φ_f of ~0.33 in THF. Knowing that the reduction potential is

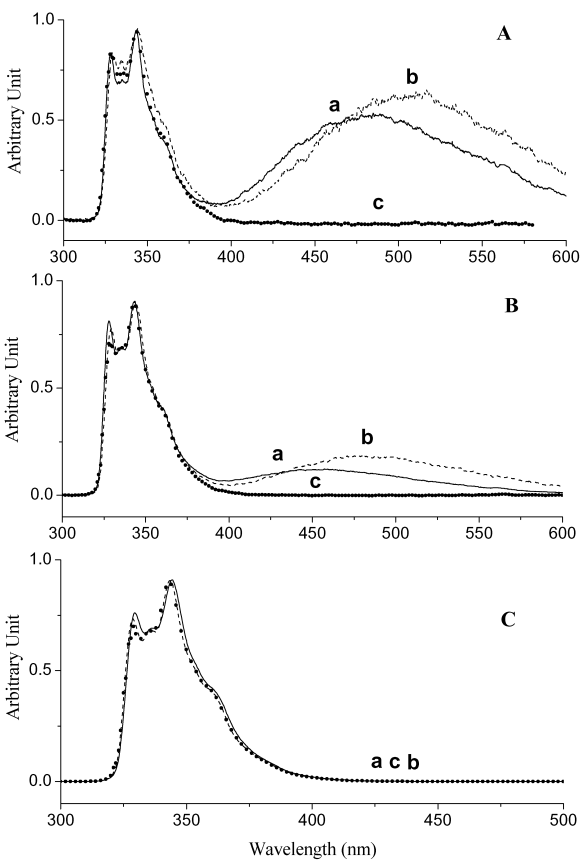

Figure 2. Fluorescence spectra of A: **2a**, B: **2b** and C: **2c** in THF (a —), DCM (b - -), and ACN (c ···). Note the intensity of spectra is in arbitrary units and has been normalized at the F_1 band peak wavelength of ~330 nm.

in the order of dicyanoethylene (−2.14 V)>ethyl 2-cyanoacetate(−2.23 V)>diethyl malonate(−2.57 V) (referred to SCE, vide infra), the results lead us to conclude that the drastic radiationless deactivation of the F_1 band in **2a** and **2b** is dominated by the photoinduced electron transfer reaction via a through-σ-bond interaction, resulting in a CT emission band.

The broad and weak CT band that originates from the charge separated D^+-A^- species can be further supported by its strong solvent-polarity dependent properties.

The spectral shift of the fluorescence upon increasing solvent polarity (Δf) depends on the difference in permanent dipole moments between ground and excited states, which can be quantitatively expressed as[33]

$$\tilde{\nu}_f = \tilde{\nu}_f^{vac} - (2|\vec{\mu}_e - \vec{\mu}_g|^2/hca_0^3)\Delta f \quad (1)$$

where $\tilde{\nu}_f$ and $\tilde{\nu}_f^{vac}$ are the spectral position (in wavenumber) of the solvation equilibrated fluorescence maxima and the value extrapolated to the gas-phase, respectively, a_0 denotes the radius of solute with a spherical cavity, μ[arrow accent]$_g$ and μ[arrow accent]$_e$ are the dipole moment vectors of the ground and excited states. Δf is the Lippert solvent polarity parameter generally expressed as: $\Delta f=(\varepsilon-1)/(2\varepsilon+1)-(n^2-1)/(2n^2+1)$, where ε and n denote the static dielectric constant and the refractive index of the solvent, respectively. The plot of $\tilde{\nu}_f$ versus Δf is sufficiently linear, in which a slope of as large as 17300 cm^{-1} is deduced for the CT band of **2a** (see Fig. 3). In contrast, the peak frequencies of the locally excited band (the F_1 band) reveal nearly solvent independence with a slope calculated to be as small as ~183 cm^{-1}.

Similar results were observed in catechol moiety series **1a-c** consisting of the same electron accepting groups as those of compound **2** series. Dual emission was resolved for **1a-c** in THF and DCM (see Fig. 4). In comparison to **5**, which is treated as a nonelectron-transfer model for **1a-c**, significant quenching of the F_1 band was also observed in **1a-c**. The quenching efficiency, indicated by the apparent F_1 fluorescence quantum yield (Table 1), is more effective in series **1a-c** than those in **2a-c**. The difference between these two categories can be rationalized qualitatively by the higher energy of LUMO for cetachol (**5**) than that of naphthanlen-

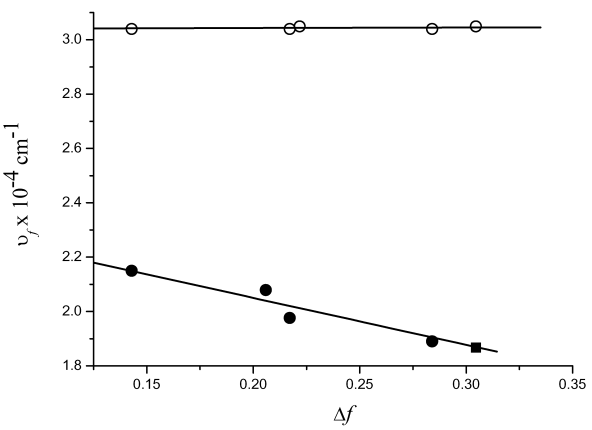

Figure 3. The plot of F_1 (○) and CT (●) peak frequencies for **2a** as a function of solvent-polarity parameter Δf. ■ denotes the predicted peak frequency of the CT band in ACN.

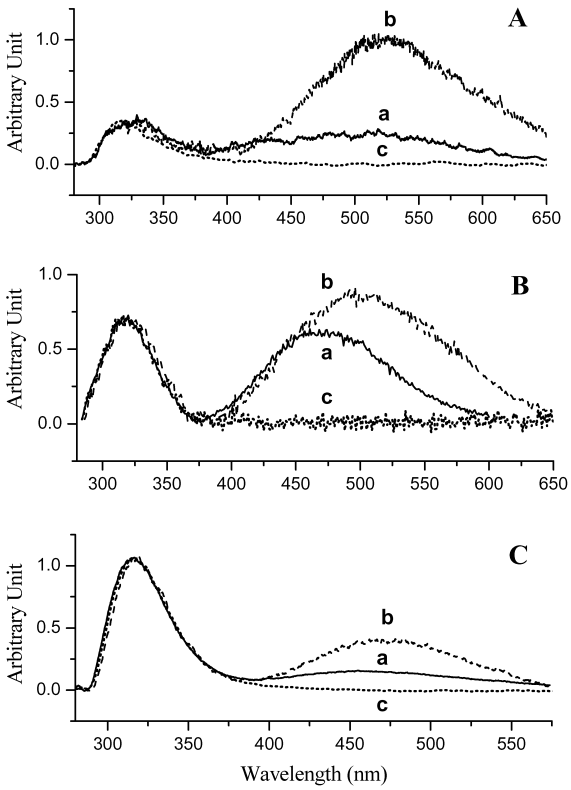

Figure 4. Fluorescence spectra of A: **1a**, B: **1b** and C: **1c** in THF (a —), DCM (b - -), and ACN (c ···). Note the intensity of spectra is in arbitrary units and has been normalized at the F_1 band peak wavelength of ~315 nm.

diol (**7**), resulting in a faster electron transfer rate for **1a-c** (vide infra).

2.2. Time-resolved electron transfer dynamics

Due to the very weak F_1 intensity, any emission caused by traces of the precursor impurity may significantly interfere with steady-state analyses. Furthermore, without the assistance of dynamic analyses, the correlation between the CT band and D/A as well as solvent properties cannot be rationalized straightforwardly by steady state approaches. For example, the electron transfer process is presumably operative for **2a** in ACN due to the significant quenching of the F_1 intensity (Φ_f~3.57×10^{-3}). According to the linear peak frequency-versus-Δf plot shown in Figure 3, the peak wavelength for the CT band is expected to be at ~533 nm for **2a** in ACN. However, the CT band was too weak to be resolved. Further time-resolved approaches are necessary to clarify this issue.

Dynamic studies were performed by a picosecond time-correlated photon counting system (see Section 5). In this section, compound **2a** will be used as a prototype throughout the discussion, followed by a brief description for the remaining D–B–A systems. For **2a** in THF the F_1 band revealed single exponential decay kinetics with a lifetime fitted to be 105 ps (χ^2=1.055, see Fig. 5). In comparison, the relaxation dynamics of the CT band could not be described solely by a single decay component. Instead, it was well fitted by dual exponential kinetics expressed as $F_2(t)=a_1 e^{-k_1 t}+a_2 e^{-k_2 t}$. Applying the convolution method, k_1 and k_2 were extracted to be 9.1×10^9 and

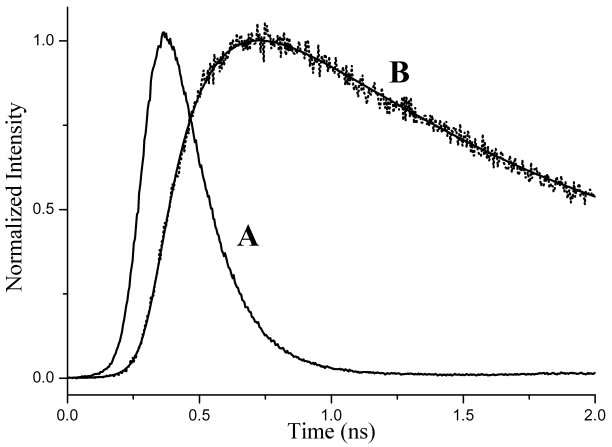

Figure 5. (A) The time-dependent fluorescence decay dynamics of **2a** monitored at the F_1 band (340 nm) in THF. (B) The rise and decay dynamics of the CT band (500 nm) associated with the fitting curve.

$5.9\times10^8\ s^{-1}$ ($\chi^2\sim1.014$, see Fig. 5). Further analyses revealed that $|a_1/a_2|$ was independent of wavelength at >450 nm and was nearly equal to 1.0. While the absolute magnitudes for a_1 and a_2 are identical, their signs are opposite with negative and positive symbols for k_1 and k_2, respectively. Furthermore, the τ_1 value ($=1/k_1$) of 110 ps in THF, within experimental error, is identical to the decay time extracted from the F_1 band (see Table 2). The results unambiguously conclude the resolvable rise dynamics for the CT band, and its origin is apparently from the F_1 band, i.e. from the vertical excitation of the naphthalendiol chromophore.

Theoretically, the observed decay rate k_{obs} of the F_1 band can be expressed as $k_{obs}=k_r+k_{nr}+k_{nr}(T)+k_{et}$ where k_{et} and k_r denote the electron transfer and radiative decay rates, respectively. k_{nr} and $k_{nr}(T)$ represent the radiationless decay rate constants, possibly involving internal conversion, intersystem crossing, etc. and temperature dependent nonradiative processes, respectively. Due to the same donor moiety and connected spacer it is reasonable to assume that $k_r+k_{nr}+k_{nr}(T)$ for **2a-c** is the same as that for **7** measured to be e.g. $9.3\times10^7\ s^{-1}$ ($\tau_{obs}=10.7$ ns) in THF. Similar procedures can be made for **1a-c** with respect to **5** of which the decay rate was measured to be $3.4\times10^8\ s^{-1}$ ($\tau_f\sim2.90$ ns) in THF. Accordingly, k_{et} values for the D–B–A systems studied in various solvents were calculated and listed in Table 2.

As shown in Table 2, the relaxation dynamics for both F_1 and CT bands are solvent-polarity dependent. For **2a** in THF and DCM the rise time of the CT band correlates very well with respect to the decay time of the F_1 band. Conversely, unlike the dual emission observed in THF and DCM, a unique F_1 band was observed for **2a** in ACN in the steady state approach (see Fig. 2(C)). The decay of the F_1 band was measured to be as fast as 71 ps, reconfirming the operation of the photoinduced electron transfer process in ACN. Expecting the peak of CT band to be ~533 nm (vide supra) for **2a** in ACN, a combination of filters was then used to isolate the emission of >520 nm in an attempt to extract the CT band. As a result, a time-resolved fluorescence signal attributed to the CT band was indeed obtained for **2a** in ACN. While its rise time was beyond the system response of 15 ps, a single exponential decay was resolved to be ~63 ps, which within experimental error is identical with the lifetime of the F_1 band.

The results can be rationalized by a time-dependent CT band expressed as

$$CT(t)=\frac{\alpha k_r^{CT}(\tilde{\nu})k_{et}[F_1]_0}{k_{CT}-k_{F_1}-k_{et}}[e^{-(k_{F_1}+k_{et})t}-e^{-k_{CT}t}] \quad (2)$$

where α denotes the instrument factor, including sensitivity, alignment, etc. of the detecting system, $[F_1]_0$ is the initial population of the normal species in the excited state, $k_r^{CT}(\tilde{\nu})$ is the radiative decay rate of the CT band at a specified wavenumber, k_{F1} is the decay rate of the F_1 band excluded the rate of electron transfer reaction, and k_{CT} denotes the observed decay rate of the CT band.[33c] It is reasonable to assume k_{et} to be $\gg k_{F1}$ for **1a-c** and **2a-b** series in ACN. As a result, Eq. (2) can be simplified to

$$CT(t)=\frac{\alpha k_r^{CT}(\tilde{\nu})k_{et}[F_1]_0}{k_{CT}-k_{et}}[e^{-k_{et}t}-e^{-k_{CT}t}] \quad (3)$$

The experimental results led us to propose that the decay of the CT band in ACN is exclusively dominated by the rate of radiationless deactivation, i.e. k_{CT}, which is even faster than k_{et}. As a result, kinetic analyses indicate that the rise time resulting from the electron transfer of ~63 ps becomes the observed decay component of the CT band in Eq. (3). On the contrary, the fast decay rate of the CT species is reflected in the irresolvable rise component of the CT band in ACN. In other words, in ACN the concentration of the excited CT species is negligibly small and possibly reaches a steady-state approximation.

The dominant quenching of the excited-state CT species by increasing the polar environment is not uncommon, especially in protic solvents like alcohols and water where the ultrafast radiationless transition is generally observed for the CT emission.[34] Dramatic polarity effects for the nonradiative CT state (charge separated form)$\rightarrow S_0$ (neutral form) back electron transfer have been reported in several systems.[35]In addition, as the local excitation (LE)-CT zero-order gap increases by increasing the solvent polarity, the radiative decay rate of the CT band, k_r^{CT} (see Eq. (3)), decreases accordingly due to the reduction in LE/CT interaction, and hence a larger fraction of the forbidden transition. The strong solvent dependence suggests that most of the radiative rate for the CT species in moderately polar solvents seems to be due to LE-CT mixing.[36] The small k_r^{CT} in combination with the fast rate of the radiationless transition rationalizes the lack of observing CT emission in ACN via the steady state approach. A similar trend was obtained for **1a-c**. However, in comparison to **2a-c** the larger exergonic CT reaction in **1a-c** leads to a faster rate of the photoinduced CT process, resulting in fast decay and rise dynamics for F_1 and CT bands, respectively. The results are consistent with the fluorescence quenching studies in the steady state approach (see Tables 1 and 2 for comparison).

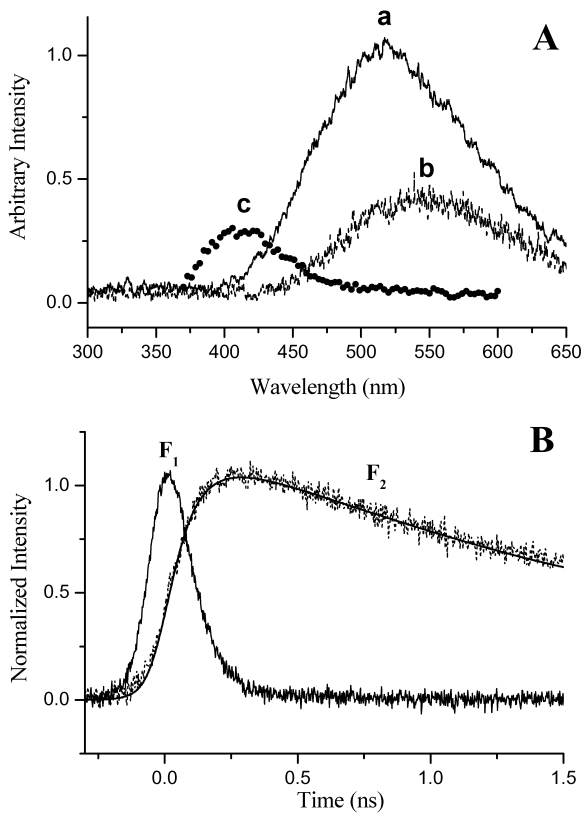

Figure 6. (A) The emission spectra of **3a** in THF (a —) and DCM (b - -), and **3b** in THF (c ···). (B)The relaxation dynamics of F_1 (370 nm) and CT (500 nm) band (F_2) for **3a** in THF.

2.3. Orientation effect between 3a and 3b

An intriguing case is the comparative study between **3a** and **3b** in which the π-orbitals orientation between benzendithiol (donor) and dicyanoethylene (acceptor) moieties are either parallel (**3a**) or perpendicular (**3b**). In the steady state approach, **3a** exhibits a very weak normal emission (i.e. the F_1 band, λ_{max}~365 nm), accompanied by a large Stokes shifted emission maximized at ~518 nm (see Fig. 6). Because the decay rate of the F_1 band for **3a** is equivalent to the corresponding rise dynamics of the 518-nm band of $\sim 4.3\times10^{10}$ s^{-1} (see Table 2), excited-state electron transfer is apparently operative in THF. In contrast, except for a very weak normal emission (i.e. the F_1 band) maximum at ~410 nm in THF, no emission band of >450 nm attributed to the CT emission could be resolved for **3b**.

While the steady state approach indicates the prohibition of the CT reaction, the decay rate of the F_1 band for **3b** was measured to be as fast as 1.0×10^{10} s^{-1} in THF. The results may be rationalized via a comparative study between **9** and **11**, the nonelectron-transfer models for compound **3a** and **3b**, respectively. In contrast to the high fluorescence yields for nonelectron-transfer models **5** and **7**, **9** and **11** exhibit very weak normal emission maxima at ~360 and 410 nm, of which the decay rates were measured to be 1.1×10^{10} and 9.3×10^{9} s^{-1}, respectively. Taking the decay dynamics of **9** and **11** to be equivalent to k_r+k_{nr} terms for **3a** and **3b**, the rates of electron transfer were thus estimated to be 3.9×10^{10} and 7×10^{8} s^{-1}, respectively. For **3b**, the relatively slow CT rate in comparison to other nonradiative decay rates leads to negligible electron-transfer efficiency (≤7%).

The intrinsic fast decay rate for **9** and **11** in combination with a very weak normal emission led us to tentatively propose that similar to benzene-1,2-dithiol,[37] the lowest excited singlet state for **9** and **11** possesses a $^1n\pi^*$ configuration. The fast depopulation of the $^1n\pi^*$ state may first be rationalized by the fast rate of $^1n\pi^*\rightarrow{}^3\pi\pi^*$ intersystem crossing (ISC). In an extreme case, through the mixing of the proximal $^1n\pi^*$ and $^1\pi\pi^*$ states the corresponding pseudo Jahn–Teller distortion may be incorporated by, enhancing a nonradiative decay channel. Such a mechanism has been proposed to explain the dominant nonradiative pathways in many chromophores possessing $^1n\pi^*/^1\pi\pi^*$ state-mixing characters.[38] Thus, competitive deactivation pathways between CT and ISC are expected for both **3a** and **3b**. According to this approach, the electron coupling matrix in the $S_{n\pi^*}$ configuration should be different from those in the **1** and **2** series possessing a pure $^1\pi\pi^*$ moiety in the lowest excited singlet state. However, the mixing $^1\pi\pi^*/^1n\pi^*$ configuration does not seem to be the main retarding factor for **3b** since appreciable CT efficiency still takes place in **3a**. Although the length of spacer in **3b** is slightly longer in distance than that in **3a** (see Fig. 1), the key difference in k_{et} is believed to be in the electron-coupling matrix resulting from the orientation between donor and acceptor moieties. The quantitative differentiation in the electron-coupling matrix between **3a** and **3b** may require detailed insights incorporating the vibronic coupling, by which the symmetry constrain can be partially removed. Focus on this approach was not engaged in this study.

3. Discussion

According to Marcus theory[39] the rate of electron transfer can be expressed as

$$k_{et} = \frac{2\pi}{(4\pi\lambda k_B T)^{1/2}\hbar}|H_{el}|^2 \exp\left[\frac{-(\Delta G^0+\lambda)^2}{4\lambda k_B T}\right] \quad (4)$$

where $|H_{el}|$ represents the electron-coupling matrix, λ denotes the nuclear reorganization energy, ΔG^0 is the reaction free energy and can be obtained from Eq. (5) expressed as

$$\Delta G^0 = E_{ox} - E_{red} - E_{00} - \frac{e^2}{4\pi\varepsilon_0} \times\left\{\left(\frac{1}{2r_D}+\frac{1}{2r_A}\right)\left(\frac{1}{\varepsilon_{ref}}-\frac{1}{\varepsilon_s}\right)-\frac{1}{\varepsilon_s d_{cc}}\right\} \quad (5)$$

where E_{ox} and E_{red} are the donor oxidation potential and the acceptor reduction potential, respectively, in a reference solvent (ACN) with a static dielectric constant ε_{ref} of 37.5, E_{00} denotes the absorption 0–0 onset of the electron donor moiety, r_D and r_A are radii of the donor and acceptor, respectively, ε_s denotes the static dielectric constant, d_{cc} symbolizes the center-to-center distance between the donor and acceptor and as revealed by X-ray structure analyses. To apply Eq. (5), r_D and r_A were estimated by a semi-empirical AM1 method by assuming a spherical cavity for both donor

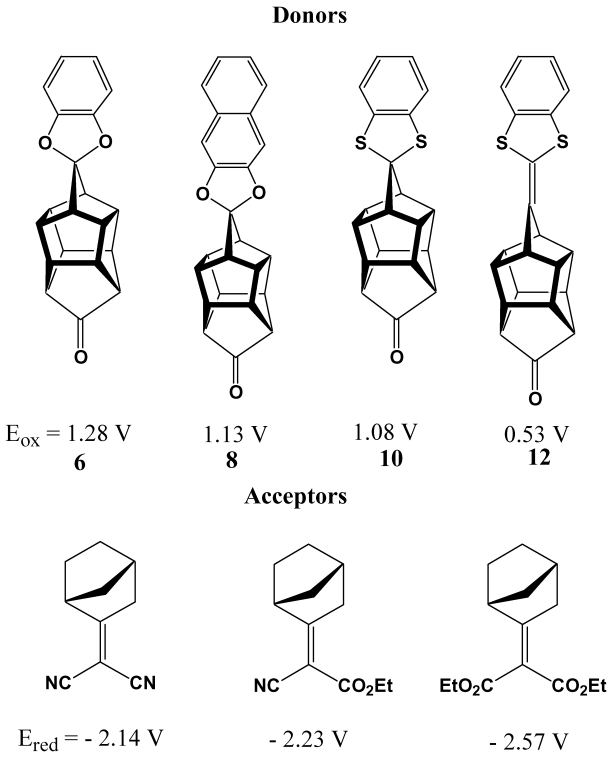

Scheme 2. Structures and redox potentials of the donors and acceptors used in this study. The redox potentials are all referred to SCE, in acetonitrile.

and acceptor. In order to obtain precise ΔG^0 values, prototypical compounds possessing only a donor-spacer or acceptor-spacer without the electron-transfer counterpart were applied, of which the structures and their corresponding redox potentials measured in ACN are depicted in Scheme 2.

Figure 7 shows a plot of k_{et} versus the reaction free energy ΔG^0 for the **1a-c** and **2a-c** series in THF. Excluding the data for **3b**, the best nonlinear least squares fit of Figure 7 using Eq. (4) gives H_{el} and λ values to be 17.3 cm^{-1} and 0.94 eV, respectively. It should be noted, however, that this tentative fitting procedure is only qualitative. Large uncertainty and hence errors might be introduced due to the assumption of unified parameters for H_{el} and λ among the studied D–B–A systems. Although the bond length of the spacer remains

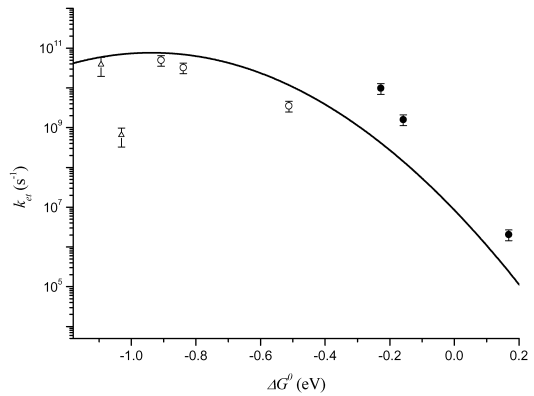

Figure 7. Plot of semi-log electron transfer rate constant, k_{et}, against ΔG^0 in THF (see Table 2). (○), (●) and (△) represents compounds **1**, **2** and **3** series, respectively. Solid line is a least squares fit of the Marcus theory (see Eq. (3)). Fit parameters (H_{el}, λ) THF (17.3 cm^{-1}, 0.94 eV).

constant, it is an oversimplification to assume the same electronic coupling factor H_{el}. Other factors incorporating configurations such as $^1n\pi^*$ and $^1\pi\pi^*$ mixing in the case of **3a** and **3b**, symmetry factors, orientations, etc. between two chromophores may tune the magnitude of H_{el}.[40] Furthermore, nuclear reorganization energy, to a certain extent, may alter among different donors and acceptors.

Nevertheless, the applied fitting procedure is still sufficiently justified on the basis of a qualitative approach. In principle, λ incorporates the solvent reorganization energy, λ_v, and the bond reorganization energy of the reactant, λ_s, expressed as[39]

$$\lambda_s = \frac{e^2}{4\pi\varepsilon_0}\left(\frac{1}{2r_D^+} + \frac{1}{2r_A^-} - \frac{1}{d_{cc}}\right)\left(\frac{1}{\varepsilon_{op}} - \frac{1}{\varepsilon_s}\right) \quad (6)$$

$$\lambda_v = \Delta G^0 + E_{00} - h\nu_{CT} - \lambda_s \quad (7)$$

where ε_{op} denotes the high-frequency optical dielectric constant ($=n_D^2$), $h\nu_{CT}$ represents the emission maximum peak frequency of the CT band. On the basis of experimental results (e.g. E_{00}, ε_{op}, ε_s, etc.) in combination with the semi-empirical approaches (r_D, r_A, d, etc.), λ_s and λ_v for the case of **2a** were calculated to be 0.71 and 0.27 eV, respectively in THF. The sum of these two parts deduces a λ value of 0.98 eV, which is only slightly different from that obtained from the curve fitting of 0.94 eV.

An attempt was also made to estimate H_{el} of back electron transfer from the relationship expressed as $k_r = \nu^2|er|^2$ in which ν is the frequency (cm^{-1}) of the CT-transition maximum. $|er|$ denotes the transition moment and is equivalent to $ed_{cc}H_{el}/(E_g - E_{CT})$ where $(E_g - E_{CT})$ specifies the energy difference between ground and charge-transfer states.[41] k_r could be extracted from $k_r = \Phi_f \times k_{CT}$ with Φ_f and k_{CT} values provided in Table 2. The calculated H_{el} values for D–B–A systems were generally an order of magnitude larger than the 17.3 cm^{-1} obtained from the Marcus theory fit. However, one should note that the Marcus theory fit provides the coupling between the locally excited state and the CT state, while from the approach of the CT radiative decay rate, one in principle derives the coupling between the ground state and the CT state. Because of the conformational rigidity and high symmetry of these D–B–A systems those couplings may be very different.[42] Focus on this issue is currently in progress.

Finally, for a given dyad, values of k_{et} show weak dependence as a function of the solvent polarity. This is expected for a forward electron transfer process, in which the generation of a charge-separated state is from an initially neutral species. In contrast, due to the generation of a neutral species via a charge-separated state, dramatic polarity effects on the excited CT state$\rightarrow S_0$ back electron transfer rate and hence the quenching of fluorescence of the CT emission are predicted, as has been discussed in ACN.

4. Conclusion

In conclusion, we have synthesized and demonstrated a new class of electron donor–{saturated hydrocarbon

bridge}–acceptor (D–B–A) dyads. The results render valuable information on the dynamics of excited-state electron transfer as functions of donor/acceptor electronic properties as well as solvent polarities. Orientation effect was also demonstrated via syntheses of **3a** and **3b** in which the electron transfer efficiency is drastically reduced in **3b** due to the 90° dihedral angle of the π-orbitals between donor and acceptor. Certainly, **3a** and **3b** may not be ideal systems for the orientation tuning studies due to their potential for mixing $^1n\pi^*$ and $^1\pi\pi^*$ characters in the lowest excited singlet state. Unfortunately, an attempt to synthesize the **3a/3b** related pair systems based on the ketal linkage was not successful at this stage.

In this study, the k_{et}-versus-ΔG^0 plot for **1a-c** and **2a-c** seems to be located within the normal Marcus types of reaction behavior, in which the rate of electron transfer increases as ΔG^0 decreases. A particular interest will be the case where the reaction is highly exergonic causing the interaction of the DA and D^+A^- to locate at the Marcus 'inverted region', i.e. the reaction gets slower with increasing exergonicity. Further rational design and syntheses of D/A chromophores as well as linear, rigid spacers aimed at the fine-tuning photoinduced electron-transfer process is currently in progress.

5. Experimental

5.1. General information

^1H and ^{13}C spectra were obtained on a Bruker APX-400 spectrometer. Mass spectra were carried out on a VG70-250S spectrometer. Infrared spectra were recorded on a Perkin–Elmer 682 infrared spectrophotometer. Elemental analyses were obtained on a Perkin–Elmer 2400 CHN instrument. Melting points were measured with a Thomas–Hoover mp apparatus and are uncorrected. Cyclic voltammetry measurements were performed using a voltammetric analyzer and a glassy-carbon working electrode in acetonitrile containing 0.1 M tetra-*n*-butylammonium tetrafluoroborate as a supporting electrolyte. Semiempirical calculations were performed by a Spartan package (Release 3.1.6, Wavefunction, Inc. Irvine, 1994) on a SiliconGraphics workstation.

5.2. Spectral analyses

Steady-state absorption and emission spectra were recorded by a Hitachi (U-3310) spectrophotometer and an Edinburgh (FS920) fluorimeter, respectively. Details of picosecond dynamical measurements have been elaborated in the previous report.[43] Briefly, the setup consists of a femtosecond Ti-Sapphire oscillator (82 MHz, Spectra Physics). The fundamental train of pulses was pulse-selected (Neos, model N17389) to reduce its repetition rate down to typically 0.8–8 MHz, and then used to produce third harmonics (260–275 nm) as an excitation light source. A polarizer was placed in the emission path to ensure that the polarization of the fluorescence was set at the magic angle (54.7°) with respect to that of the pump laser to eliminate the fluorescence anisotropy. An Edinburgh OB 900-L time-correlated single photon counting system was used as a detecting system. The time-dependent fluorescence data were analyzed by the sum of exponential functions incorporating the excitation-pulse profile with an iterative convolution,[44] which allows partial removal of the instrument time broadening and consequently renders a temporal resolution of ~15 ps.

THF, DCM, ACN and cyclohexane (Merck Inc.) were all of spectragrade quality. To prevent the water perturbation originating from the moisture, except for cyclohexane, solvents were refluxed several hours under a nitrogen atmosphere and were transferred, prior to use, though distillation to the sample cell. Samples were degassed by three freeze-pump-thaw cycles in vacuo. Fluorescence quantum yields were measured using diluted 7-azaindole ($<1\times10^{-5}$ M in cyclohexane) as reference, assuming a yield of 0.22 with 280 nm excitation.[45] For determining the yield of CT band, 7-methyl-7*H*-pyrrolo[2,3]pyridine was used as a reference for which the fluorescence yield was measured to be 5.2×10^{-3} upon 300 nm excitation.[43]

5.3. Synthesis

5.3.1. 7-Dicyanomethylidene-12-heptacyclo[6.6.0.0^{2,6}.0^{3,13}.0^{4,11}.0^{5,9}.0^{10,14}]tetradecanone monocatechol ketal (1a). A round-bottom flask equipped with a Dean–Stark apparatus and a condenser was charged with **6** (98 mg, 0.33 mmol), malononitrile (135 mg, 2.04 mmol), glacial acetic acid (0.33 mL), β-alanine (70 mg, 0.79 mmol), and freshly distilled benzene (25 mL) under a nitrogen atmosphere. The solution was refluxed for 15 h, and quenched by the addition of saturated K_2CO_3 solution. The resulting mixture was extracted several times with ethyl acetate. The combined organic layer was washed several times with brine, dried over anhydrous $MgSO_4$, filtered, and concentrated in vacuo. The residue was purified by a silica gel chromatography eluted with solvent mixture of dichloromethane and hexane. Compound **1a** was collected as white solid (105 mg, 0.31 mmol) in 93% yield; mp 345°C (decomp.). IR (KBr) 2982, 2225, 1629, 1488 cm^{-1}; ^1H NMR (300 MHz, $CDCl_3$) δ 2.65 (s, 2H), 2.86 (s, 4H), 3.06 (s, 4H), 3.25 (s, 2H), 6.72–6.80 (m, 4H); ^{13}C NMR (75 MHz, $CDCl_3$) δ 52.13, 52.44, 52.56, 53.94, 75.48, 109.01, 112.18, 122.01, 135.73, 148.01, 196.72; *m/z* (%) 352 (M^+, 100%), 315 (4), 274 (6), 247 (20), 231 (40).

5.3.2. 7-Cyano(ethoxycarbonyl)methylidene-12-heptacyclo[6.6.0.0^{2,6}.0^{3,13}.0^{4,11}.0^{5,9}.0^{10,14}]tetradecanone monocatechol ketal (1b). Preparation from **6** was similar to that of **1a**. White solid (75% yield); mp 270–271°C. IR (KBr) 2976, 2224, 1734, 1641, 1485 cm^{-1}; ^1H NMR (300 MHz, $CDCl_3$) δ 1.35 (t, 3H, *J*=7.0 Hz), 2.62 (bs, 2H), 2.80 (bs, 4H), 3.01 (bs, 4H), 3.23 (bs, 1H), 4.00 (bs, 1H), 4.28 (q, 2H, *J*=7.0 Hz), 6.77–6.80 (m, 4H); ^{13}C NMR (75 MHz, $CDCl_3$) δ 14.11, 48.78, 51.12, 51.56, 51.91, 52.82, 53.17, 61.81, 94.96, 108.19, 115.19, 121.14, 135.15, 147.40, 161.61, 191.13; *m/z* (%) 399 (M^+, 100%), 371 (2), 354 (3), 326 (3), 317 (4).

5.3.3. 7-Di(ethoxycarbonyl)methylidene-12-heptacyclo[6.6.0.0^{2,6}.0^{3,13}.0^{4,11}.0^{5,9}.0^{10,14}]tetradecanone monocatechol ketal (1c). A round-bottom flask containing $TiCl_4$ (0.10 mL) and CCl_4 (0.25 mL) in THF (3.0 mL) was cooled

to 0°C under a nitrogen atmosphere. It was stirred for 30 min with a magnetic bar, then a solution of dimethyl malonate (0.01 mL) in THF (1.0 mL) was added to it dropwise, followed by a solution of **6** (21.7 mg, 0.071 mmol) in THF (1 mL), and finally pyridine (0.20 mL). The mixture was allowed to gradually warm to room temperature, and stirred for 17 h. It was quenched by the addition of distilled water. The resulting mixture was extracted several times with methylene chloride (100 mL total). The combined organic layer was washed several times with brine, dried over anhydrous $MgSO_4$, filtered, and concentrated in vacuo. The residue was purified by a silica gel chromatography eluted with solvent mixture of hexane and ethyl acetate (4:1 ratio). Compound **1c** was collected as white solids (24.8 mg, 0.059 mmol, 83% yield); mp 173–174°C. IR (KBr) 2987, 1719, 1663, 1482 cm^{-1}; ^1H NMR (300 MHz, $CDCl_3$) δ 1.30 (t, 6H, J=7.0 Hz), 2.59 (bs, 2H), 2.75 (bs, 4H), 2.93 (bs, 4H), 3.38 (bs, 2H), 4.24 (q, 4H, J=7.0 Hz), 6.73–6.79 (m, 4H); ^{13}C NMR (75 MHz, $CDCl_3$) δ 14.14, 49.75, 51.09, 51.64, 53.29, 60.97, 108.14, 114.72, 121.03, 135.10, 147.51, 165.22, 175.89; *m/z* (%) 446 (M^+, 100%), 401 (10), 354 (5), 328 (3), 309 (10).

5.3.4. 7-Dicyanomethylidene-12-heptacyclo[6.6.0.0^{2,6}.0^{3,13}.0^{4,11}.0^{5,9}.0^{10,14}]tetradecanone naphthalene-2,3-diol ketal (2a). Preparation of **2a** from **8** was similar to that of **1a** from **6**. White solid (94% yield); mp 281–284°C. IR (KBr) 2962, 2914, 2220, 1625 1468 cm^{-1}; ^1H NMR (300 MHz, $CDCl_3$) δ 2.68 (s, 2H), 2.89 (s, 4H), 3.11 (s, 4H), 3.27 (s, 2H), 7.04 (s, 2H), 7.30–7.33 (m, 2H), 7.63–7.66 (m, 2H); ^{13}C NMR (75 MHz, $CDCl_3$) δ 52.15, 52.50, 52.59, 54.11, 75.58, 104.21, 112.16, 124.99, 127.62, 130.99, 136.00, 148.24, 196.60; *m/z* (%) 352 (M^+, 100%), 315 (4), 274 (6), 247 (20), 231 (40).

5.3.5. 7-Cyano(ethoxycarbonyl)methylidene-12-heptacyclo[6.6.0.0^{2,6}.0^{3,13}.0^{4,11}.0^{5,9}.0^{10,14}]tetradecanone naphthalene-2,3-diol ketal (2b). Preparation of **2b** from **8** was similar to that of **1a** from **6**. White solid (93% yield); mp 255–256°C. IR (KBr) 2970, 2224, 1729, 1651, 1469 cm^{-1}; ^1H NMR (300 MHz, $CDCl_3$) δ 1.33 (t, 3H, J=7.1 Hz), 2.61 (bs, 2H), 2.79 (bs, 4H), 3.04 (bs, 4H), 3.21 (bs, 1H), 3.99 (bs, 1H), 4.26 (q, 2H, J=7.1 Hz), 7.01 (s, 2H), 7.25–7.30 (m, 2H), 7.59–7.62 (m, 2H); ^{13}C NMR (75 MHz, $CDCl_3$) δ 14.13, 48.82, 51.18, 51.63, 51.97, 52.86, 53.36, 61.86, 95.07, 103.37, 115.19, 124.16, 126.87, 130.27, 135.46, 147.69, 161.62, 191.01; *m/z* (%) 449 (M^+, 67%), 421 (2), 404 (1), 377 (7), 354 (100).

5.3.6. 7-Di(ethoxycarbonyl)methylidene-12-heptocyclo-[6.6.0.0^{2,6}.0^{3,13}.0^{4,11}.0^{5,9}.0^{10,14}]tetradecanone naphthalene-2,3-diol ketal (2c). Preparation of **2c** from **8** was similar to that of **1c** from **6**. Compound **2c** was collected as white solids in 97% yield; mp 182–183°C. IR (KBr) 2980, 1720, 1670, 1473 cm^{-1}; ^1H NMR (300 MHz, $CDCl_3$) δ 1.31 (t, 6H, J=7.1 Hz), 2.61 (bs, 2H), 2.77 (bs, 4H), 2.98 (bs, 4H), 3.40 (bs, 2H), 4.25 (q, 4H, J=7.1 Hz), 7.03 (s, 2H), 7.27–7.31 (m, 2H), 7.61–7.65 (m, 2H); ^{13}C NMR (75 MHz, $CDCl_3$) δ 14.16, 49.80, 51.18, 51.70, 53.49, 61.00, 103.28, 114.85, 124.08, 126.84, 130.28, 135.44, 147.84, 165.22, 175.76; *m/z* (%) 496 (M^+, 100%), 451 (7), 424 (2), 378 (2).

5.3.7. 7-Dicyanomethylidene-12-heptocyclo[6.6.0.0^{2,6}.0^{3,13}.0^{4,11}.0^{5,9}.0^{10,14}]tetradecanone benzene-1,2-dithiol ketal (3a). A round-bottom flask equipped with a Dean–Stark apparatus and a condenser was charged with **10** (80 mg, 0.24 mmol), malononitrile (112 mg, 1.70 mmol), glacial acetic acid (0.27 mL), β-alanine (58 mg, 0.65 mmol), and freshly distilled benzene (25 mL) under a nitrogen atmosphere. The solution was refluxed for 20 h, and quenched by the addition of saturated K_2CO_3 solution. The resulting mixture was extracted several times with ethyl acetate. The combined organic layer was washed several times with brine, dried over anhydrous $MgSO_4$, filtered, and concentrated in vacuo. The residue was purified by a silica gel chromatography eluted with a solvent mixture of dichloromethane and hexane. Compound **3a** was collected as white solid (85 mg, 92% yield). Mp 341°C (decomp.). IR (KBr) 2971, 2230, 1637, 1446 cm^{-1}; ^1H NMR (300 MHz, $CDCl_3$) δ 2.82 (s, 4H), 2.99 (s, 2H), 3.09 (s, 4H), 3.27 (s, 2H), 7.00–7.02 (m, 2H), 7.14–7.17 (m, 2H); ^{13}C NMR (75 MHz, $CDCl_3$) δ 51.93, 53.62, 55.06, 60.23, 75.46, 87.30, 112.09, 122.97, 126.14, 138.02, 195.64 *m/z* (%) 384 (M^+, 65%), 347 (6), 330 (10), 315 (25). Anal. calcd for $C_{23}H_{16}N_2S_2$: C, 71.84, H, 4.19; found: C, 71.79, H, 4.12.

5.3.8. 7-(1′,3′-Benzodithiolylidene)-12-(dicyanomethylidene)heptacyclo[6.6.0.0^{2,6}.0^{3,13}.0^{4,11}.0^{5,9}.0^{10,14}]tetradecane (3b). Preparation of **3b** from **12** was similar to that of **3a** from **10**. Compound **3b** was collected as white solid in 93% yield. Mp 337°C (decomp.). IR (KBr) 2966, 2230, 1662, 1630 cm^{-1}; ^1H NMR (300 MHz, $CDCl_3$) δ 2.75 (s, 4H), 2.88 (s, 2H), 2.92 (s, 2H), 3.24 (s, 2H), 6.94–6.70 (m, 2H), 7.05–7.11 (m, 2H); ^{13}C NMR (75 MHz, $CDCl_3$) δ 51.95, 53.16, 53.35, 55.30, 75.14, 112.17, 114.46, 122.09, 126.23, 136.86, 142.37 *m/z* (%) 396 (M^+, 100%), 347 (4), 330 (4), 315 (10).

5.3.9. 12-Hydroxyheptacyclo[6.6.0.0^{2,6}.0^{3,13}.0^{4,11}.0^{5,9}.0^{10,14}]tetradecan-7-one catechol ketal (5). A round-bottom flask, equipped with a Dean–Stark apparatus was charged with **4** (362 mg, 1.69 mmol), catechol (186 mg, 1.69 mmol), and *p*-toluenesulfonic acid (20 mg, 0.12 mmol) in benzene (100 mL) under a nitrogen atmosphere. The reaction was heated to reflux for 12 h. It was quenched by the addition of saturated Na_2CO_3 solution. The organic layer was extracted several times with ether, washed with brine, and dried over anhydrous $MgSO_4$. It was filtered and the filtrate was concentrated in vacuo. The residue was purified by silica gel column chromatography eluted with a mixture of CH_2Cl_2 and hexane. Compound **5** was collected as white solids (484 mg, yield 94%); mp 199–200°C. IR (KBr) 3255, 2462, 1484, 1328 cm^{-1}; ^1H NMR (300 MHz, $CDCl_3$) δ 2.38 (s, 2H), 2.45 (s, 1H), 2.55 (s, 2H), 2.62 (s, 1H), 2.81 (s, 4H), 2.94 (s, 2H), 4.58 (s, 1H), 6.75–6.76 (m, 4H); ^{13}C NMR (75 MHz, $CDCl_3$) δ 50.15, 50.72, 52.43, 53.14, 54.35, 55.67, 87.47, 108.78, 121.57, 135.41, 148.38; *m/z* (%) 307 (20, M^++1), 306 (100, M^+), 211 (5), 197 (5), 178 (15). Anal. calcd for $C_{20}H_{18}O_3$: C, 78.41, H, 5.92; found: C, 78.34, H, 6.05.

5.3.10. Heptacyclo[6.6.0.0^{2,6}.0^{3,13}.0^{4,11}.0^{5,9}.0^{10,14}]tetradecan-7,12-dione monocatechol ketal (6). A round-bottom flask equipped with a N_2 adapter was charged with **5** (250 mg, 0.82 mmol) in freshly distilled CH_2Cl_2 (10 mL), followed by pyridinium chlorochromate (PCC, 530 mg,

2.45 mmol). The reaction mixture was stirred at room temperature for 3 h, and then filtered. The filtrate was concentrated, and applied onto a silica gel chromatography eluted with a solvent mixture (50% each) of ethyl acetate and hexane. Compound **6** was collected as white powder (222 mg, 0.73 mmol) in 89% yield; mp 271–272°C. IR (KBr) 2983, 1760, 1628, 1596, 1483 cm^{-1}; ^1H NMR (300 MHz, $CDCl_3$) δ 2.40 (s, 2H), 2.53 (s, 2H), 2.73 (s, 4H), 3.04 (s, 4H), 6.77 (s, 4H); ^{13}C NMR (75 MHz, $CDCl_3$) δ 47.24, 50.66, 51.26, 52.34, 108.23, 121.19, 135.47, 147.54, 216.09; *m/z* (%) 304 (64, M^+), 231 (50), 215 (30).

5.3.11. 12-Hydroxyheptacyclo[6.6.0.0^{2,6}.0^{3,13}.0^{4,11}.0^{5,9}.0^{10,14}]tetradecan-7-one naphthalene-2,3-diol ketal (7). A similar procedure for the preparation of **5** was utilized. Compound **7** was obtained from **4** in 96% yields. Physical data of **7**: IR (KBr) 3237, 2961, 1627, 1600, 1484, 1326 cm^{-1}; δ_H ($CDCl_3$, 300 MHz) 2.41 (s, 2H), 2.45 (s, 1H), 2.55 (s, 2H), 2.62 (s, 1H), 2.84 (s, 4H), 2.94 (s, 2H), 4.58 (s, 1H), 7.00 (s, 2H), 7.24–7.29 (m, 2H), 7.60–7.63 (m, 2H); δ_C ($CDCl_3$, 75 MHz, ^1H-decoupled) 50.22, 50.73, 50.79, 52.47, 53.32, 54.37, 55.86, 87.52, 103.87, 124.67, 127.50, 130.97, 135.77, 145.12; *m/z* (EI) 356 (M^+, 5%), 329 (10), 307 (27), 289 (15), 176 (20), 154 (100), 136 (68).

5.3.12. Heptacyclo[6.6.0.0^{2,6}.0^{3,13}.0^{4,11}.0^{5,9}.0^{10,14}]tetradecan-7,12-dione mononaphthalene-2,3-diol ketal (8). The oxidation reaction was completed following the same procedures as that of **6** from **5**. Ketone **8** was obtained from **7** in 87% yields. Mp 228–229°C. IR (KBr) 2970, 1765, 1474, 1325 cm^{-1}; δ_H ($CDCl_3$, 300 MHz) 2.43–2.44 (m, 2H), 2.55–2.56 (m, 2H), 2.76 (br, 4H), 3.09 (br, 4H), 7.05 (s, 2H), 7.29–7.32 (m, 2H), 7.63–7.66 (m, 2H); δ_C ($CDCl_3$, 75 MHz, ^1H-decoupled) 47.91, 51.47, 51.94, 53.04, 104.08, 124.85, 127.57, 130.99, 136.41, 148.45, 216.78; *m/z* (EI) 356 (M^+, 5%), 329 (10), 307 (27), 289 (15), 176 (20), 154 (100), 136 (68).

5.3.13. 12-Hydroxyheptacyclo[6.6.0.0^{2,6}.0^{3,13}.0^{4,11}.0^{5,9}.0^{10,14}]tetradecan-7-one benzene-1,2-dithiol ketal (9). A round-bottom flask, equipped with a Dean–Stark apparatus was charged with **4** (200 mg, 0.93 mmol), catechol (133 mg, 0.93 mmol), and *p*-toluenesulfonic acid (16 mg, 0.093 mmol) in toluene (65 mL) under a nitrogen atmosphere. The reaction was heated to reflux for 10 h. It was quenched by the addition of saturated Na_2CO_3 solution. The organic layer was extracted several times with ether, washed with brine, and dried over anhydrous $MgSO_4$. It was filtered and the filtrate was concentrated in vacuo. The residue was purified by silica gel column chromatography eluted with a mixture of $CHCl_3$ and hexane. Compound **9** was collected as white solids (295 mg, yield 93%); mp 186–187°C. IR (KBr) 3300, 2958, 2883, 1565, 1443, 1343 cm^{-1}; ^1H NMR (300 MHz, $CDCl_3$) δ 2.42 (s, 2H), 2.50 (s, 2H), 2.79 (s, 1H), 2.83 (s, 4H), 2.88 (s, 2H), 2.94 (s, 1H), 4.50 (s, 1H), 6.96–6.99 (m, 2H), 7.13–7.15 (m, 2H); ^{13}C NMR (75 MHz, $CDCl_3$) δ 50.19, 51.83, 52.68, 53.22, 55.90, 59.71, 62.11, 85.33, 86.16, 122.79, 125.74, 138.61; *m/z* (%) 338 (37, M^+), 290 (4), 256 (8), 213 (5), 178 (40). Anal. calcd for $C_{20}H_{18}S_2O$: C, 70.97, H, 5.36; found: C, 71.01, H, 5.24.

5.3.14. Heptacyclo[6.6.0.0^{2,6}.0^{3,13}.0^{4,11}.0^{5,9}.0^{10,14}]tetradecan-7,12-dione monobenzene-1,2-dithiol ketal (10). A round-bottom flask equipped with a N_2 adapter was charged with **9** (200 mg, 0.59 mmol) in freshly distilled CH_2Cl_2 (10 mL), followed by pyridinium chlorochromate (PCC, 383 mg, 1.78 mmol). The reaction mixture was stirred at room temperature for 3 h, and then was filtered. The filtrate was concentrated, and applied onto a silica gel chromatography eluted with a solvent mixture (1:4 by volume) of ethyl acetate and hexane. Compound **10** was collected as white solid (147 mg, 74% yields). Mp 228–229°C. IR (KBr) 2987, 2952, 1760, 1563, 1444 cm^{-1}; ^1H NMR (300 MHz, $CDCl_3$) δ 2.40 (s, 2H), 2.68 (s, 4H), 2.86 (s, 4H), 3.07 (s, 2H), 6.96–7.01 (m, 2H), 7.11–7.17 (m, 2H); ^{13}C NMR (75 MHz, $CDCl_3$) δ 47.41, 53.32, 55.71, 57.63, 87.59, 122.86, 125.99, 138.25, 216.47; *m/z* (%) 336 (16, M^+), 256 (8), 236 (7). Anal. calcd for $C_{20}H_{16}S_2O$: C, 71.39, H, 4.79; found: C, 71.45, H, 4.62.

5.3.15. 7-(1′,3′-Benzodithiolylidene)-12-heptacyclo-[6.6.0.0^{2,6}.0^{3,13}.0^{4,11}.0^{5,9}.0^{10,14}]tetradecanol (11). Compounds **11** and **12** were synthesized by the method developed by Ishikawa et al.[46] with slight modification. To a solution of diethyl 1,3-benzodithiolylphosphonate (160 mg, 0.56 mmol) in THF (15 mL) was added *n*-BuLi in hexane (0.40 mL of 1.6 M, 0.64 mmol) at −78°C under nitrogen with stirring. The solution turned to orange-red. A solution of **4** (120 mg, 0.56 mmol) in THF (5 mL) was then added after 10 min and the mixture turned to yellow. It was stirred for another 10 min at −78°C, then water (25 mL) was added to it. The mixture was extracted with dichloromethane (3×50 mL), dried over anhydrous $MgSO_4$, filtered, and concentrated in vacuo. The residue was recrystallized from THF and hexane as white solid (162 mg, 83% yield). Mp 256–257°C. IR (KBr) 3336, 2960, 2876, 1666, 1567, 1448 cm^{-1}; ^1H NMR (300 MHz, $CDCl_3$) δ 2.39 (s, 2H), 2.44 (s, 2H), 2.62 (s, 4H), 2.72 (br, 1H), 2.83 (s, 2H), 2.90 (br, 1H), 4.50 (s, 1H), 6.94–7.00 (m, 2H), 7.04–7.11 (m, 2H); ^{13}C NMR (75 MHz, $CDCl_3$) δ 49.65, 51.28, 51.93, 52.26, 52.73, 54.41, 54.85, 86.39, 121.28, 125.27, 136.60, 142.74; *m/z* (%) 350 (12, M^+), 306 (6), 256 (8), 236 (5), 213 (5). Anal. calcd for $C_{21}H_{18}S_2O$: C, 71.96, H, 5.18; found: C, 72.09, H, 5.16.

5.3.16. 7-(1′,3′-Benzodithiolylidene)-12-heptacyclo-[6.6.0.0^{2,6}.0^{3,13}.0^{4,11}.0^{5,9}.0^{10,14}]tetradecanone (12). To a solution of diethyl 1,3-benzodithiolylphosphonate (684 mg, 2.36 mmol) in THF (60 mL) *n*-BuLi in hexane (1.5 mL of 1.6 M, 2.4 mmol) was added at −78°C under nitrogen with stirring. The solution turned to orange-red. A solution of HCTD-7, 12-dione (500 mg, 2.36 mmol) in THF (20 mL) was added after 10 min, and the mixture turned to yellow. It was stirred for another 10 min at −78°C, and then water (25 mL) was added to it. The mixture was extracted with dichloromethane (3×50 mL), dried over anhydrous $MgSO_4$, filtered, and concentrated in vacuo. The residue was resolved by a silica gel chromatography eluted with a solvent mixture of ethyl acetate and hexane (1:10). Compound **12** was collected as white solid (89 mg, 22% yield), along with un-reacted dione (245 mg) and a doubly reacted side product (452 mg). Mp 267–268°C. IR (KBr) 2963, 1770, 1447 cm^{-1}; ^1H NMR (300 MHz, $CDCl_3$) δ 2.30 (s, 2H), 2.54 (s, 4H), 2.70 (s, 2H), 2.78 (br, 2H), 6.91–6.95 (m, 2H), 6.97–7.02 (m, 2H); ^{13}C NMR (75 MHz, $CDCl_3$) δ 46.79, 49.91, 52.54, 55.25, 112.42, 121.40, 125.50, 136.44,

1443.26, 216.64; *m/z* (%) 348 (4, M^+), 278 (3), 264 (4), 257 (16), 255 (14). Anal. calcd for $C_{21}H_{16}S_2O$: C, 72.38, H, 4.63; found: C, 72.33, H, 4.50.

Acknowledgements

This work was supported by the National Science Council NSC (90-2113-M-002-055). The authors are also grateful to Emeritus Professor N. -C. Yang of the University of Chicago for helpful discussion.

References

1. Creed, D.; Caldwell, R. A. *Photochem. Photobiol.* **1985**, *180*, 715–739.
2. Gray, H. B.; Winkler, J. R. *Annu. Rev. Biochem.* **1996**, *65*, 537–561, and references therein.
3. Larsson, S. *Biochim. Biophys. Acta, Bioenerg.* **1998**, *1365*, 294–300.
4. Slate, C. A.; Striplin, D. R.; Moss, J. A.; Chen, P.; Ericson, B. W.; Meyer, T. J. *J. Am. Chem. Soc.* **1998**, *120*, 4885–4886.
5. Treadway, J. A.; Chem, P. Y.; Rutherford, T. J.; Keene, F. R.; Meyer, T. J. *J. Phys. Chem. A* **1997**, *101*, 6824–6826.
6. Ashton, P. R.; Ballardini, R.; Balzani, V.; Constable, E. C.; Credi, A.; Kocian, D.; Langford, S. J.; Preece, J. A.; Prodi, L.; Schofield, E. R.; Spencer, N. *Chem-Eur. J.* **1998**, *12*, 2413–2422.
7. Park, J. W.; Lee, B. A.; Lee, S. Y. *J. Phys. Chem. B* **1998**, *102*, 8209–8215.
8. Thorton, N. B.; Wojtowicz, H.; Netzel, T.; Dixon, D. W. *J. Phys. Chem. B* **1998**, *102*, 2101–2110.
9. Balzani, V.; Juris, A.; Venturi, M. *Chem. Rev.* **1996**, *96*, 759–834, and references therein.
10. Di Bilio, A. J.; Dennison, C.; Gray, H. B.; Ramirez, B. E.; Sykes, A. G.; Winkler, J. R. *J. Am. Chem. Soc.* **1998**, *120*, 7551–7556.
11. Skov, L. K.; Pascher, T.; Winkler, J. R.; Gray, H. B. *J. Am. Chem. Soc.* **1998**, *120*, 1102–1103.
12. Speiser, S. *Chem. Rev.* **1996**, *96*, 1953–1976, and references therein.
13. (a) Oliver, A. M.; Black, A. J.; Craig, D. C.; Paddon-Row, M. N. *Langmuir* **1996**, *12*, 6616–6626. (b) Roest, M. R.; Verhoeven, J. W.; Schuddeboom, W.; Warman, J. M.; Lawson, J. M.; Paddon-Row, M. N. *J. Am. Chem. Soc.* **1996**, *118*, 1762–1768. (c) Lawson, J. M.; Oliver, A. M.; Rothenfluh, D. F.; An, Y. Z.; Ellis, G. A.; Ranasinghe, M. G.; Khan, S. I.; Franz, A. G.; Ganapathi, P. S.; Shephard, M. J.; Paddon-Row, M. N.; Rubin, Y. *J. Org. Chem.* **1996**, *61*, 5032–5054. (d) Williams, R. M.; Koeberg, M.; Lawson, J. M.; An, Y. Z.; Rubin, Y.; Paddon-Row, M. N.; Verhoeven, J. W. *J. Org. Chem.* **1996**, *61*, 5055–5062. (e) Roest, M. R.; Oliver, A. M.; Paddon-Row, M. N.; Verhoeven, J. W. *J. Phys. Chem. A* **1997**, *101*, 4867–4871. (f) Craig, D. C.; Ghiggino, K. P.; Jolliffe, K. A.; Langford, S. J.; Paddon-Row, M. N. *J. Org. Chem.* **1997**, *62*, 2381–2386. (g) Gulyas, P. T.; Langford, S. J.; Lokan, N. R.; Ranasinghe, M. G.; Paddon-Row, M. N. *J. Org. Chem.* **1997**, *62*, 3038–3039. (h) Jones, G. A.; Carpenter, B. K.; Paddon-Row, M. N. *J. Am. Chem. Soc.* **1998**, *120*, 5499–5508. (i) Wegewijs, B.; Paddon-Row, M. N.; Braslavsky, S. E. *J. Phys. Chem. A* **1998**, *102*, 8812–8818. (j) Lokan, N.; Paddon-Row, M. N.; Smith, T. A.; Rosa, M. L.; Ghiggino, K. P.; Speiser, S. *J. Am. Chem. Soc.* **1999**, *121*, 2917–2918. (k) Jones, G. A.; Carpenter, B. K.; Paddon-Row, M. N. *J. Am. Chem. Soc.* **1999**, *121*, 11171–11178. (l) Shephard, M. J.; Paddon-Row, M. N. *J. Phys. Chem. A* **1999**, *103*, 3347–3350.
14. Tung, C. H.; Zhang, L. P.; Li, Y.; Cao, H.; Tanimoto, Y. *J. Am. Chem. Soc.* **1997**, *119*, 5348–5354.
15. Agyin, J. K.; Timberlake, L. D.; Morrison, H. *J. Am. Chem. Soc.* **1997**, *119*, 7945–7953.
16. Portela, C. F.; Brunckova, J.; Richards, J. L.; Schöllhorn, B.; Iamomoto, Y.; Magde, D.; Traylor, T. G.; Perrin, C. L. *J. Phys. Chem. A* **1999**, *103*, 10540–10552.
17. MacMahon, S.; Fong, R., II.; Baran, P. S.; Safonov, I.; Wilson, S. R.; Schuster, D. I. *J. Org. Chem.* **2001**, *66*, 5449–5455.
18. Metzger, R. M. *J. Mater. Chem.* **2000**, *10*, 55–62.
19. Scheib, S.; Cava, M. P.; Baldwin, J. W.; Metzger, R. M. *J. Org. Chem.* **1998**, *63*, 1198–1204.
20. Langer, J. J.; Martynski, M. *Syn. Met.* **1999**, *107*, 1–6.
21. Aviram, A.; Ratner, M. A. *Chem. Phys. Lett.* **1974**, *29*, 277–283.
22. Chen, J.; Reed, M. A.; Rawlett, A. M.; Tour, J. M. *Science* **1999**, *286*, 1550–1552.
23. de Silva, A. P.; Gunaratne, H. Q. N.; Gunnlaugsson, T.; Huxley, A. J. M.; McCoy, C. P.; Rademacher, J. T.; Rice, T. E. *Chem. Rev.* **1997**, *97*, 1515–1566.
24. Yu, C. J.; Chong, Y.; Kayyem, J. F.; Gozin, M. *J. Org. Chem.* **1999**, *64*, 2070–2079.
25. Lewis, F. D.; Wu, T.; Zhang, Y.; Letsinger, R. L.; Greenfield, S. R.; Wasielewski, M. R. *Science* **1997**, *277*, 673–676.
26. Gust, D.; Moore, T. A.; Moore, A. L. *Acc. Chem. Res.* **1992**, *26*, 198–205.
27. Boyd, R. W. *Nonlinear Optics*; Academic: New York, 1992.
28. Prasad, P. N.; Williams, D. J. *Introduction to Nonlinear Optical Effects in Molecular and Polymers*; Wiley: New York, 1991.
29. Wasielewski, M. *Chem. Rev.* **1992**, *92*, 435–461.
30. Balzani, V.; Juris, A.; Venturi, M. *Chem. Rev.* **1996**, *96*, 759–834.
31. Chiou, N. R.; Chow, T. J.; Chen, C. Y.; Hsu, M. A.; Chen, H. C. *Tetrahedron Lett.* **2001**, *42*, 29–31.
32. Chow, T. J.; Hon, Y. S.; Chen, C. Y.; Huang, M. S. *Tetrahedron Lett.* **1999**, *40*, 7799–7801.
33. (a) Lippert, V. Z. *Electrochemistry* **1957**, *61*, 652–975. (b) Matage, N.; Kaifu, Y.; Koizumi, M. *Bull. Chem. Soc. Jpn* **1956**, *29*, 465–470. (c) Chapman, C. F.; Maroncelli, M. *J. Phys. Chem.* **1956**, *96*, 8430–8441.
34. For example, see: Chou, P. T.; Chang, C. P.; Clements, J. H.; Kuo, M. S. *J. Fluorescence* **1995**, *5*, 369–375.
35. For example, see: (a) Hopfield, J. J. *Protein Structure: Molecular and Electronic Reactivity*; Springer: New York, 1987. (b) Joran, A. D.; Leland, B. A.; Felker, P. M.; Zewail, A. H.; Hopfield, J. J.; Dervan, P. B. *Nature* **1987**, *327*, 508–511.
36. Kang, T. J.; Kahlow, M. A.; Giser, D.; Swallen, S.; Nagarajan, V.; Jarzeba, W.; Barbara, P. F. *J. Phys. Chem.* **1988**, *92*, 6800–6807.
37. Chou, P. T.; Yu, W. S. Unpublished results.
38. Lim, E. C. *J. Phys. Chem.* **1986**, *90*, 6770–6777.
39. (a) Marcus, R. A. *J. Chem. Phys.* **1965**, *43*, 679–701. (b) Marcus, R. A. *Annu. Rev. Phys. Chem.* **1964**, *15*, 155–196. (c) Marcus, R. A. *J. Chem. Phys.* **1956**, *424*, 966. (d) Marcus, R. A. *Discuss. Faraday Soc.* **1960**, *29*, 21.

(e) Marcus, R. A.; Sutin, N. *Biochim. Biophys. Acta* **1985**, *811*, 275.

40. (a) Heiler, D.; McLendon, G.; Rogalskyj, P. *J. Am. Chem. Soc.* **1987**, *109*, 604–606. (b) Miller, J. R.; Calcaterra, L. T.; Closs, G. L. *J. Am. Chem. Soc.* **1984**, *106*, 3047–3049. (c) Closs, G. L.; Calcaterra, L. T.; Green, N. J.; Penfield, K.; Miller, J. R. *J. Phys. Chem.* **1986**, *90*, 3673–3683. (d) Closs, G. L.; Miller, J. R. *Science* **1988**, *240*, 440–447. (e) Closs, G. L.; Johnson, M. D.; Miller, J. R.; Piotrowiak, P. *J. Am. Chem. Soc.* **1989**, *111*, 3751–3753. (f) Liang, N.; Miller, J. R.; Closs, G. L. *J. Am. Chem. Soc.* **1989**, *111*, 8740–8741. (g) Rettig, W.; Gleiter, R. *J. Phys. Chem.* **1985**, *89*, 4676–4680.
41. (a) Oevering, H.; Verhoeven, J. W.; Paddon-Row, M. N.; Warman, J. M. *Tetrahedron* **1989**, *45*, 4751–4766. (b) Bixon, *J. Am. Chem. Soc.* **1994**, *116*, 7349–7355.
42. (a) Zeng, Y.; Zimmt, M. B. *J. Am. Chem. Soc.* **1991**, *113*, 5107–5109. (b) Zeng, Y.; Zimmt, M. B. *J. Phys. Chem.* **1992**, *96*, 8395–8403. (c) Kumar, K.; Tepper, R. J.; Zeng, Y.; Zimmt, M. B. *J. Org. Chem.* **1995**, *60*, 4051–4066.
43. Chou, P. T.; Chen, Y. C.; Yu, W. S.; Chou, Y. H.; Wei, C. Y.; Cheng, Y. M. *J. Phys. Chem. A* **2001**, *105*, 1731–1740.
44. Demas, J. N.; Crosby, G. A. *J. Phys. Chem.* **1971**, *75*, 991–1024.
45. Chapman, C. F.; Maroncelli, M. *J. Phys. Chem.* **1992**, *96*, 8430–8441.
46. (a) Ishikawa, K.; Akiba, K.-y.; Inamoto, N. *Tetrahedron Lett.* **1976**, *41*, 3695–3698. (b) Akiba, K.-y.; Ishikawa, K.; Inamoto, N. *Synthesis* **1977**, 861–862.